Research Square

Preprints are preliminary reports that have not undergone peer review.
They should not be considered conclusive, used to inform clinical practice,
or referenced by the media as validated information.

Hydraulic performance and vibration response of a centrifugal pump with a 3D-printed impeller under controlled unbalance conditions

Daniel Emilio Casagrande

daniel.casagrande@uoh.cl

Universidad de O'Higgins https://orcid.org/0000-0001-9579-9801

Sebastián Daniel Jeldres Sepúlveda

Universidad de O'Higgins

Luis Enrique Ortiz-Vidal

Universidad Tecnologica del Peru https://orcid.org/0000-0001-6924-7552

Research Article

Keywords: Additive manufacturing, Impeller unbalance, Centrifugal pump, Dynamic response, Vibration analysis

Posted Date: November 20th, 2026

DOI: https://doi.org/10.21203/rs.3.rs-11625811/v1

License: This work is licensed under a Creative Commons Attribution 4.0 International License.
Read Full License

Hydraulic performance and vibration response of a centrifugal pump with a 3D-printed impeller under controlled unbalance conditions

Daniel Emilio Casagrande[1], Sebastián Daniel Jeldres Sepúlveda[1], Luis Enrique Ortiz-Vidal[2*]

[1]Institute of Engineering Sciences, Universidad de O'Higgins, Rancagua, Chile.

[2]Facultad de Ingeniería de Sistemas y Electrónica, Universidad Tecnológica del Perú, Lima, Perú.

*Corresponding author(s). E-mail(s): C30057@utp.edu.pe, enrique.ortizvidal@outlook.com;
Contributing authors: daniel.casagrande@uoh.cl; sebastian.jeldres@uoh.cl;

Abstract

Centrifugal pump performance and reliability can be strongly affected by rotor unbalance, while the increasing use of additive manufacturing raises additional questions related to the dynamic behavior of printed rotating components. This study experimentally investigates the hydraulic performance and vibration response of a centrifugal pump equipped with a fused deposition modeling (FDM) impeller manufactured from polylactic acid (PLA) and subjected to controlled added-mass conditions. The hydraulic performance of the 3D-printed impeller was first compared with that of the original impeller through head–flow rate and vibration measurements, showing similar overall behavior, with an average difference of approximately 4% between the head–flow rate curves. A controlled unbalance was then introduced by adding masses at a fixed radial position of up to 0.270 g, corresponding to an added unbalance magnitude approximately three times the calculated permissible residual unbalance reference, without removing the impeller from the shaft. Five 15-second vibration measurements were recorded for each condition in both radial and axial directions, and the corresponding power spectral densities (PSD) were analyzed. The vibration response was dominated by the 3X rotational component rather than the expected 1X component. Moreover, the 3X peak PSD amplitude initially decreased with added mass and

subsequently increased, which may indicate partial compensation of an existing unbalance of the rotor assembly before additional mass increased the overall unbalance. The dominant 3X response may be associated with structural resonance or the dynamic characteristics of the partially infilled FDM impeller. These results demonstrate the feasibility of using additively manufactured impellers for controlled experimental studies of pump unbalance and vibration behavior.

Keywords: Additive manufacturing; Impeller unbalance; Centrifugal pump; Dynamic response; Vibration analysis

1 Introduction

Centrifugal pumps are essential for fluid transportation in many industries, including but not limited to oil and mining, chemical, food production and water management industries. Centrifugal pumps are the most widely used, with a market size that surpassed 1 billion USD in 2023 and is expected to reach 1.5 billion USD in 2032 according to Business Research Insights and other market-analysis reports. The rise is attributed to the surge in oil and gas production as well as the increasing demand in food and chemical industries and in water treatment plants. It is also expected that in the coming years, new technologies will be integrated into pumps, such as Internet-of-Things (IoT)-based monitoring technologies, to reduce failures and increase performance [1–3].

The performance of these pumps is highly dependent on design (impeller type, material selection, etc), operational conditions (operating point, cavitation and vibration, etc) and on the application (fluid characteristics, industry-specific needs, etc) [4–7]. Excessive vibrations in particular can occur for several reasons: mechanical and/or hydraulic unbalance, mechanical issues (such as shaft misalignment, seal or bearing defects, inadequate piping supports or foundation), fluid-induced vibration or hydraulic disturbances (such as cavitation, air entrainment, hydraulic resonance) and other mechanical problems such as structural resonance (an operating speed close to, or capable of exciting a natural frequency of the structure) [8–13]. While in the short term high levels of vibration can lead to increased noise and reduced performance, in the long term they can lead to premature failure of the pump or piping structure [4, 7, 10].

The most common technique used for predictive maintenance of static structures and rotating machinery is vibration analysis [14]. Vibration analysis is used to monitor the condition of structures and machinery and detect faults [4, 14, 15]. In [16], the authors present a review of vibrations that occur in different turbomachines, including pumps, introducing their causes and effects. They classify the causes of vibration in pumps into three main categories: hydraulic (vaporization of liquid, insufficient clearance between impeller and pump cutwater, air entrapment, turbulence and water hammer), mechanical (unbalanced rotating components, damaged impellers, shaft deflection, misalignments, inadequate pump foundation, thermal stress and friction due to rubbing parts) and peripheral causes (harmonic vibration from nearby equipment, pump operation at a critical speed, and seal faces temporarily seizing).

Mechanical mass unbalance and hydraulic unbalance are two major factors affecting pump vibration [10]. The mechanical unbalance of a rotor or shaft in rotary machines can be classified into static and couple unbalance components. Static unbalance can be defined as the eccentricity of the center of mass of a rotor, and it can be represented by an equivalent point mass at a certain radius from the rotation axis of the rotor. Static balancing deals with resolving forces in one plane and adding a correction mass at a specific radius in that plane [17, 18]. Rotors with mass concentrated near a single transverse plane (i.e., a rotor diameter greater than 7 to 10 times its width) can be treated as static balancing problems, such as flywheels, car wheels, certain impellers, etc. [17, 18]. Couple or moment unbalance can be found in rotors whose diameter is less than 7 to 10 times its width and balancing it involves vibration measurements and the addition of correction masses in two planes [17, 18]. Hydraulic unbalance can also generate forces that have effects similar to those of mechanical unbalance [10]. Mechanical and hydraulic unbalance, as well as other sources of vibration, can be diagnosed by analyzing the spectrum of vibration signals using accelerometers at specific positions [4, 5, 11, 19, 20].

The impellers of centrifugal pumps are produced using conventional manufacturing tools. Nonetheless, the advances in 3D-printing technologies have enabled the transition of many industries from traditional manufacturing processes to 3D printing, not only for rapid prototyping purposes but also for the design and production of complex parts [21]. In recent years, research interest has increased in the use of additive manufacturing technology to fabricate impellers [22–36].

The performance of various 3D-printed impellers is compared with that of a traditional iron impeller in [22]. The authors conducted tests on impellers made of ABS, PLA, HIPS, and carbon fiber, assessing stress, performance, and efficiency. Their results show that a PLA impeller with a 60% infill exhibits similar characteristics to those of a cast iron impeller. Similarly, in [23], two 3D-printed impellers, with and without post-treatment to reduce surface roughness, were compared with the original impeller of a centrifugal pump. The impellers were designed as replicas of the original steel impeller of the pump, and were printed using ABS. Similar head-flow-rate curves were obtained for the considered impellers, with slightly better performance overall of the chemically post-treated 3D-printed impeller for high-flow-rate operating conditions. The study presented in [24] deals with the comparison of five impellers with identical geometry: cast iron, steel, composite (ABS + cast iron), shell (ABS), full (ABS). The first two impellers were fabricated using sand-mold casting, while the latter three were printed using ABS. Their tests show that the 3D-printed impellers achieved better efficiency at high flow rates, which the authors attributed to lower surface roughness, and highlight the feasibility of rapid fabrication of the impeller. The works presented in [25] and [26] deal with the use of reinforced polymers for the 3D printing of impellers. In [25] the authors compare the mechanical properties of four materials, two used in traditional impeller manufacturing and two used in additive manufacturing, for the impellers: cast iron alloy, brass alloy, carbon-fiber-reinforced polyamide 6 (PA6-CF15) and carbon-fiber-reinforced polyphenylene sulfide (PPS-CF15). Their simulation results show that although traditional metal impellers can withstand higher loads, the composite impellers were approved to operate up to

9.32 kW (PA6-CF15) and 4.1 kW (PPS-CF15). Furthermore, these materials are corrosion resistant, thereby reducing corrosion-related degradation, and they are highly chemically resistant. On the other hand, the focus in [26] is on the optimization of parameters for the 3D printing of impellers using graphene-reinforced PLA. The article presents optimal values for the printing parameters to achieve enhanced mechanical properties for the impeller. The work presented in [27] deals with the dynamics of a 3D-printed microrotor used in an amalgam separator. The authors used Fused Deposition Modeling (FDM) with 100% infill and they found that, because the deposited layers of material do not cover the entire cross-sectional area of the rotor, the rotor exhibits orthotropic behavior, specifically, directional differences in its second moment of inertia that grows exponentially as the shaft cross-sectional area decreases. They concluded that printing parameters are key, and that if the orthotropy level is minimum, it is expected that the rotor will exhibit subharmonic resonances and instability regions in the frequency spectrum [27]. More recently, the same authors experimentally demonstrated that infill density and raster orientation affect the harmonic content and critical speeds of ABS-FDM rotors, with lower infill densities producing increasingly prominent 2X and 3X components [37]. In [28], the authors present a 3D-printed miniature centrifugal pump for microfluidic applications that uses permanent magnets and achieves flow rates of up to 124 mL/min. The ecological footprint of CNC-machined impellers is compared with that of metal 3D-printed impellers in [29]. Their analysis indicates that metal 3D-printed impellers can offer economic and environmental advantages, under the conditions examined, compared to the traditional impeller fabricated using subtractive manufacturing [29]. A co-occurrence analysis is performed in [30] to investigate the use of additive manufacturing in turbomachinery. The authors claim that additive manufacturing offers opportunities for cost reduction and performance improvement, by replacing traditional manufacturing or integrating additive manufacturing for the fabrication of components.

The literature review shows that a 3D-printed impeller can achieve hydraulic performance comparable to that of a conventionally manufactured impeller; however, limited information is available regarding their dynamic response and vibration behavior, particularly under controlled unbalance conditions. The work presented here focuses on the use of additive manufacturing technology for the fabrication of the impeller of a centrifugal pump, and on how the use of such an impeller affects the pump in terms of its hydraulic performance and dynamic response. The study considers several added-mass conditions of the 3D-printed impeller to investigate how changes in the impeller mass distribution, such as those potentially associated with localized material loss or detachment, influence the vibration response of the pump. An experimental set-up is designed so that the centrifugal pump can be tested and monitored in a closed circuit using two accelerometers, allowing a rapid change between the original and 3D-printed impellers and, more importantly, the progressive addition of trial masses without removing the impeller from the shaft. The main contribution of this work is the experimental characterization of the hydraulic and dynamic response of a centrifugal pump using a 3D-printed impeller under controlled added-mass conditions.

The paper is structured in four sections. Section 2 describes the experimental methodology, including impeller fabrication, hydraulic testing, vibration measurements, and data analysis. Section 3 presents and discusses the hydraulic and vibration results. Finally, Section 4 summarizes the main findings and conclusions.

2 Methods

This section first describes the experimental set-up; followed by the impeller fabrication and unbalancing procedures. Finally, the data-acquisition and processing procedures are presented.

2.1 Experimental set-up

The diagram of the experimental set-up used in this study is presented in Figure 1. The test section consists of a closed-loop circuit in which water is drawn from a tank by a centrifugal pump. Pressure gauges were installed at the pump inlet and outlet, and a flow meter was installed downstream. A valve is used to regulate the flow of water passing through the test section. This arrangement also enabled the pump performance curves to be measured.

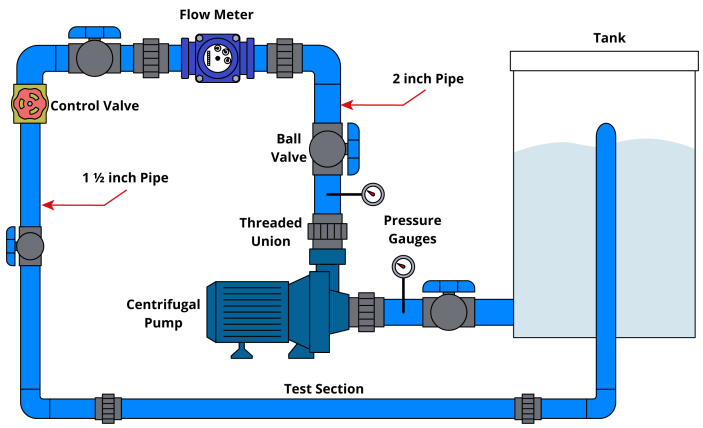


Fig. 1: Diagram of the experimental set-up.

Photographs of the test rig are presented in Figure 2. The centrifugal pumps were mounted on a metal structure in a position that allows easy assembly and disassembly to swap the impellers during tests. Only one of the centrifugal pumps was used in the experiments. The main components included Reggio® SCF1 100T centrifugal pumps (1 HP rated power, maximum flow rate of 350 L/min, nominal rotational speed of 2,850 rpm, and maximum head of 13 m); Itahydraulic® pressure gauges (pressure range: -1 to 2 bar), flow meter (measuring range: 7 to 500 L/min).



(a) Overview of the experimental set-up (b) Close-up of the centrifugal pumps

Fig. 2: Experimental set-up of the centrifugal pump system.

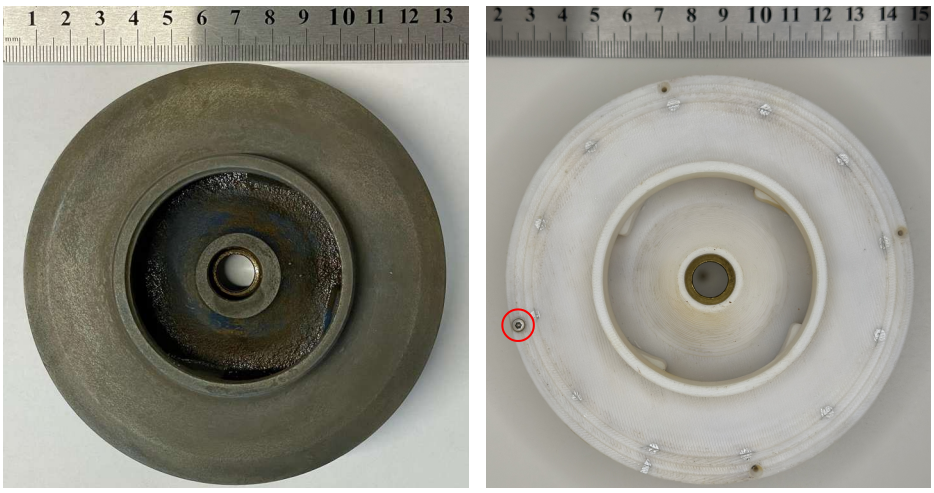
2.2 Impeller fabrication

The study explores the use of 3D printing to fabricate impellers that could be intentionally unbalanced, because printed components can be readily modified and manufactured with good repeatability. A replica of the original impeller, with four evenly spaced blades, was designed in Autodesk Fusion®. Polylactic acid (PLA) was the material chosen to fabricate the impeller due to its ease of use, low cost, and the favorable results reported by Babayiğit et al. [22], Fernández et al. [23] and Polák [24].

Figure 3 shows the front view of the original impeller and of the final version of the 3D-printed impeller, in which the four blades of the impellers can be seen. The 3D-printed impeller, shown in Figure 3b, was modified relative to the original impeller, shown in Figure 3a, to introduce unbalance. This was achieved with the addition of four equally spaced holes aligned with the blades of the impeller with the aim of symmetrically distributing the removed material and minimizing unwanted unbalance. Screws with increasing mass were installed in one of these holes, allowing different levels of added unbalance to be introduced. The four symmetrical holes near the impeller periphery can be seen in Figure 3b, with the trial-mass location highlighted by a red circle. In addition, to reduce misalignment between the impeller and the shaft, a bronze coupling insert was fitted into the 3D-printed impeller, which can be seen at the center of the impeller. Furthermore, to reduce the risk of cracking near the shaft connection, the local infill density in this region was increased to 100%.

Developing a satisfactory printed replica required several iterations. More than 30 impellers were fabricated while different printing parameters were evaluated until a satisfactory configuration was obtained using the printing settings reported in Table 1. The 3D-printed replica required approximately 6 hours to print using a Creality Ender 3 V3 SE printer.

To assess the dimensional accuracy and repeatability of the manufacturing process, five impellers fabricated using the final printing parameters were measured and compared with the original impeller. Five diameters, D1 to D5, were measured in two perpendicular directions, while the spacing H1 between the impeller walls was



(a) Original impeller (b) 3D-printed impeller

Fig. 3: Comparative view of impellers. The red circle indicates a hole used to intentionally introduce unbalance.

Table 1: 3D-printing settings for the impeller.

Parameter	Value	Unit
Layer height	0.2	mm
Infill density	60	%
Nozzle diameter	0.4	mm
Wall thickness	2.0	mm
Printing speed	180	mm/s
Temperature of the nozzle	210	°C
Temperature of the build plate	60	°C
Support pattern	Zig-Zag	-

measured at four angular positions separated by 90°. The total impeller height H2 was also measured. These dimensions are presented in Fig. 4, while Table 2 presents the original impeller dimensions, the mean and standard deviation of the five printed impellers, and the dimensions of impeller I5, which was used for the hydraulic and vibration experiments. The results show close dimensional agreement with the original impeller, with mean relative deviations below 1.2% for the dimensions reported in Table 2. Furthermore, the standard deviations across the five printed impellers ranged from 0.04 to 0.15 mm, indicating low dimensional variability between specimens under the selected manufacturing conditions. These results support the suitability of the adopted printing parameters for producing geometrically consistent impellers.

For each impeller, the two perpendicular measurements of each diameter were averaged, as were the four wall-spacing measurements. Sample standard deviations were calculated across the five impellers (I1–I5). The values are rounded to 0.01 mm

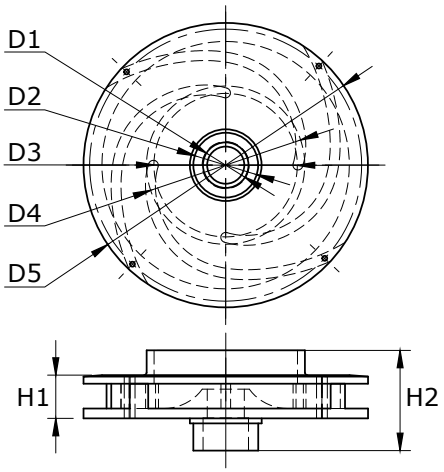


Fig. 4: Impeller dimensions D1 to D5, H1 and H2.

Table 2: Dimensional comparison between the original impeller and five FDM-manufactured impellers.

Dimension	Original [mm]	Printed mean ± SD (n=5) [mm]	I5 (tested) [mm]
D1	18.40	18.41 ± 0.08	18.45
D2	26.20	25.89 ± 0.15	25.85
D3	58.00	57.96 ± 0.04	58.00
D4	64.00	63.47 ± 0.07	63.40
D5	115.00	114.66 ± 0.10	114.80
H1	17.70	17.84 ± 0.05	17.83
H2	40.70	40.62 ± 0.08	40.60

for presentation, although the original measurements were recorded to 0.1 mm, using a digital caliper with a specified resolution of 0.01 mm and uncertainty of ± 0.02 mm.

2.3 Impeller unbalancing

After fabrication and installation of the 3D-printed impeller, controlled unbalance was introduced by installing trial masses at a fixed radial position. For reference, the permissible residual unbalance was calculated according to ISO 21940-11 using Eqs. 1 and 2.

$$U_{per} = \frac{9549}{N} \cdot G \cdot M \tag{1}$$

$$m_{per} = \frac{U_{per}}{r} \tag{2}$$

where U_{per} is the permissible residual unbalance in g · mm, m_{per} is the equivalent permissible residual-unbalance mass in g at radius r, N is the rotational speed in rpm, G is the balance quality grade in mm/s, M is the mass of the impeller in kg, and r is the radial distance to the unbalance mass in mm.

The rotational speed was measured as 2,820 rpm during a separate test, rather than simultaneously with the vibration measurements. The impeller mass was 0.09303 kg, and the trial-mass radius was 56 mm. A balance quality grade of G16 was deliberately adopted as a relatively coarse reference for defining the experimental trial-mass conditions. These parameters yielded a permissible residual unbalance U_{per} of approximately 5.04 g·mm, equivalent to a mass of 0.090 g at the specified radius.

Five experimental conditions were considered: a baseline condition without an added trial mass and four conditions with added masses of 0.135, 0.180, 0.225, and 0.270 g. These masses correspond to added unbalance magnitudes of 1.5, 2.0, 2.5, and 3.0 times the calculated permissible residual unbalance U_{per}, respectively, as summarized in Table 3. The baseline condition represents the rotor assembly without an added trial mass and does not imply zero residual unbalance. The actual residual unbalance of the assembled rotor was not measured independently.

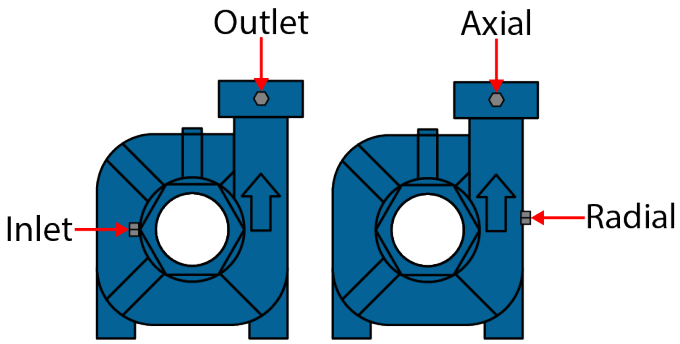
Table 3: Unbalance scenarios and added masses.

Condition	**Added mass**	**Added unbalance**	**Added unbalance relative to U_{per}**
Baseline	0.000 g	0.00 g mm	0.0
1	0.135 g	7.56 g mm	1.5
2	0.180 g	10.08 g mm	2.0
3	0.225 g	12.60 g mm	2.5
4	0.270 g	15.12 g mm	3.0

To assess installation-related geometric deviations, axial runout was measured using a dial indicator. Once the 3D-printed impeller had been installed, successive trial masses were introduced without removing it from the shaft. Only the pump front cover was removed and reinstalled between conditions.

2.4 Data acquisition and analysis

Hydraulic performance and vibration tests were performed to assess the 3D-printed impeller. The performance of the 3D-printed impeller was assessed by comparing head-flow-rate (H-Q) curves of the original impeller and of the replica. In this test, manual instrumentation was used to measure the pressure and flow rate over a flow-rate range of 0-300 L/min. Pump efficiency was calculated as the ratio of hydraulic output power to electrical input power, using the applied voltage, the current drawn by the pump, its nominal power factor, its flow rate, head and the specific gravity of water (considered equal to 1). Finally, to assess vibration levels using both impellers, PCB 352C65 accelerometers were installed at the inlet and outlet of the pump as shown in Figure 5a.



(a) Performance test (b) Unbalance test

Fig. 5: Position of the accelerometers for the assessment of the (a) performance and (b) unbalance of the 3D-printed impeller.

Following these hydraulic and vibration tests, controlled trial masses were added to the 3D-printed impeller to investigate their influence on the dynamic response of the pump. The same accelerometers were then mounted at the pump outlet in axial and radial orientations, as presented in Figure 5b. In both experiments, a dSPACE MicroLabBox was used to acquire the accelerometers signals, using a PCB 480E9 signal conditioner between the sensors and the acquisition system, as shown in Figure 6.

The accelerometer locations were selected based on configurations reported in previous centrifugal-pump vibration studies. Measurements near the inlet and outlet have been used to characterize the overall pump vibration response under different operating flow conditions [11, 19], while radial and axial vibration measurements on the pump casing or bearing region are commonly employed to characterize rotor-related dynamic behavior [11, 20].

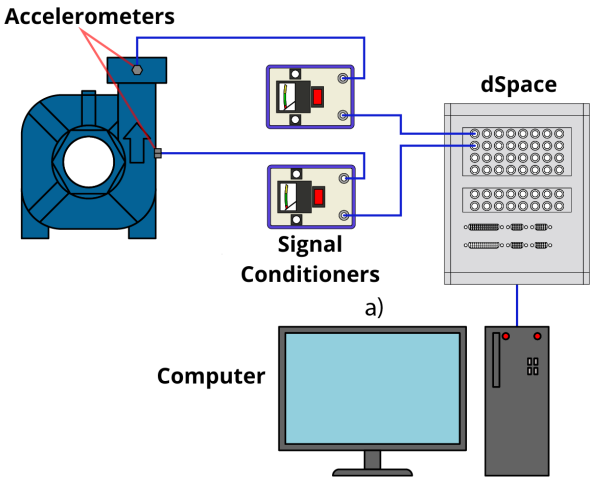


Fig. 6: Accelerometer signal-acquisition set-up.

For each trial-mass condition, the front cover of the pump was removed to install the appropriate trial mass without removing the impeller, after which the front cover was reinstalled, the pump was purged and, to allow transient effects to decay before the measurements, the pump was operated at a flow rate of approximately 293 L/min for several minutes before conducting the measurement. Five 15-s trials were recorded for each unbalance configuration, and the pump was switched off and restarted between successive trials, without removing the pump-impeller assembly. The accelerometer sampling frequency was set to 8 kHz. The resulting data were preprocessed to obtain vectors of the same length and the PSD of each vector was calculated using 1-s Hann windows with a 50% overlap. For each trial-mass condition, the PSD was estimated independently for each of the five vibration records. The mean PSD was then calculated to compare the overall spectral response across conditions. For the quantitative comparison of the presumed 1X component, the maximum PSD magnitude within the 40–60 Hz frequency band was extracted from each individual record. For the presumed 3X component, the global maximum PSD magnitude was extracted from each record, as the dominant spectral peak was observed near 147 Hz. The mean and sample standard deviation of the five extracted peak values were subsequently calculated for each trial-mass condition and measurement direction.

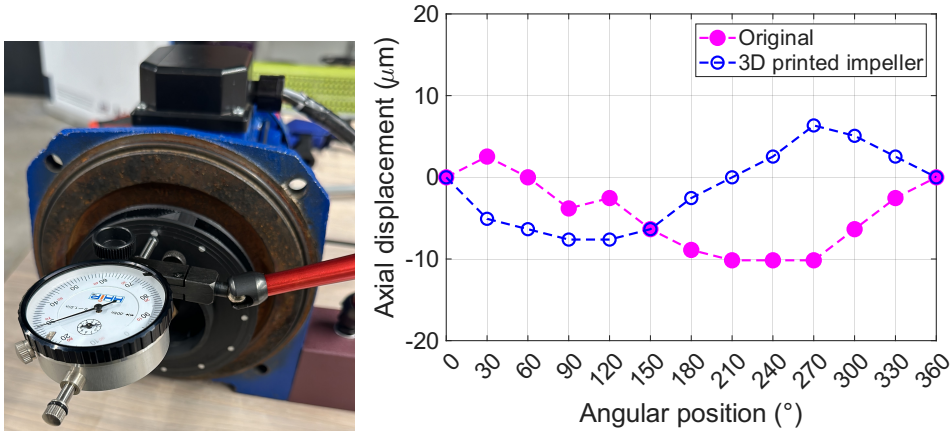
3 Results and discussion

3.1 Validation of the 3D-printed impeller

The axial runout measurements obtained using a dial indicator for the original and 3D-printed impellers are presented in Figure 7. Figure 7a shows the set-up for the dial-indicator measurement, while Figure 7b presents the readings over one complete shaft revolution, recorded at angular increments of 30°, which are indicated using markers. The total indicated runout (TIR), calculated as the difference between the maximum

and minimum discrete readings over one revolution, was 12,7 μm for the original impeller (pink line with solid round markers) and 13.97 μ for the 3D-printed impeller (blue line with hollow round markers). This suggests the installation of the 3D-printed impeller did not introduce a substantial increase in axial geometric deviation.

Figure 8 presents the head-flow-rate (H-Q) curves of the centrifugal pump obtained with the original impeller (pink line with solid round markers) and with the 3D-printed impeller (blue line with hollow round markers). The values provided by the manufacturer are also plotted here (green dashed line with cross markers) for nominal speed. The markers represent measured values, and second-order polynomials were fitted to the datasets. The impellers show similar hydraulic performance, with an average difference of approximately 4% between the two fitted curves. The original impeller produced a lower head at low flow rates. The difference diminishes as the flow rate increases up to approximately 80 L/min, where both impellers achieve the same head. At higher flow rates, the original impeller achieves a slightly higher head up to the maximum value of approximately 300 L/min, at which the maximum difference between the impellers reaches approximately 13%.



(a) Dial indicator

(b) Axial runout

Fig. 7: Axial runout of the original (pink line with solid round markers) and 3D-printed impeller (blue line with hollow round markers).

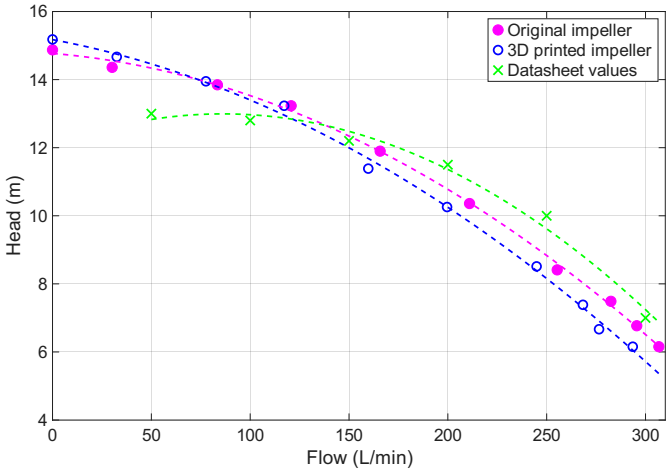
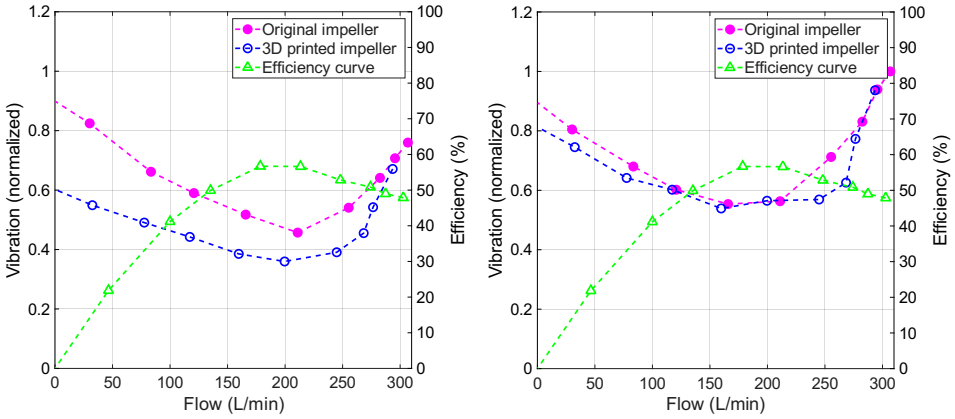


Fig. 8: H-Q curve of the pump to assess the performance using the original impeller (pink dashed line with solid markers) and the 3D-printed impeller (blue dashed line with hollow markers). The values provided by the manufacturer are also presented (green dashed line with cross markers).

Figure 9 shows the normalized acceleration measured at the inlet (a) and outlet (b) of the pump using the original impeller (dashed pink line with solid markers) and the 3D-printed impeller (dashed blue line with hollow markers). The acceleration curves were normalized with respect to the maximum value registered at the outlet using the original impeller. The efficiency of the pump using the original impeller (dashed green line with solid markers) is also shown in these two plots. The markers indicate the measured values and the lines represent second-order polynomial fits. The acceleration curves obtained with the original impeller and its replica exhibit similar trends, with the characteristic inverted bell shape: higher vibration levels at low and high flow rates with a minimum near 200 L/min. This minimum occurs in the vicinity of the highest value in the efficiency curve, characterized by a bell shape curve and which is close to the estimated BEP (Best Efficiency Point) of the pump. Measurements at the inlet of the pump show lower acceleration levels for the printed impeller, approaching those of the original impeller at the upper end of the tested flow-rate range. Measurements at the outlet of the pump show similar acceleration levels for both impellers with a broader minimum for the printed impeller, particularly at approximately 250 L/min where the amplitude is lower than for the original impeller.



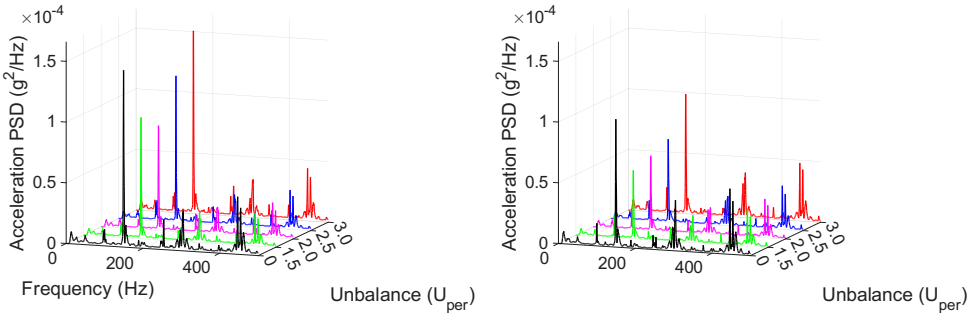
(a) Inlet (b) Outlet

Fig. 9: Normalized acceleration measured at the inlet and outlet of the pump using the original impeller (pink line with solid markers) and its replica (blue line with hollow markers) versus flow rate. The efficiency-flow-rate (E-Q) curve (green line with solid markers) of the pump is also presented.

The results presented in Figures 8 and 9 indicate that the 3D-printed impeller reproduces the overall hydraulic and vibration behavior of the original impeller with sufficient agreement to support the subsequent comparative experiments. In the next section, the 3D-printed impeller is subjected to progressively increasing trial masses to assess the corresponding dynamic response.

3.2 Dynamic response of the centrifugal pump using an unbalanced impeller

The acceleration PSDs measured in the radial and axial directions were compared with the baseline condition across the different trial-mass conditions. Figure 10 shows the results for the (a) radial and (b) axial directions for the baseline condition (no added trial mass) (black lines), and for the added trial masses that correspond to 1.5 (green lines), 2.0 (pink lines), 2.5 (blue lines), and 3.0 (red lines) times the permissible unbalance U_{per}.



(a) Radial direction (b) Axial direction

Fig. 10: PSD of the acceleration (mean value of 5 repetitions) measured in the radial and axial directions for different impeller unbalance configurations relative to the permissible unbalance U_{per}: baseline or 0 (black line), 1.5 (green line), 2.0 (pink line), 2.5 (blue line), and 3.0 (red line).

The vibration spectra show larger amplitudes near 49 Hz and its integer multiples, with the dominant peak occurring near 147 Hz. These frequencies are consistent with the first and third rotational harmonics of a shaft rotating at approximately 2,940 rpm. However, the rotational speed was not measured simultaneously with the vibration signals. The independently measured speed of 2,820 rpm was obtained during a separate test, and the difference may reflect variations in operating conditions between experiments. All vibration measurements were conducted under the same operating conditions, suggesting that the rotational speed remained approximately constant across the trial-mass conditions. Accordingly, the components near 49 and 147 Hz are hereafter referred to as the presumed 1X and 3X components, respectively.

The baseline PSD shows peak values at 1X and its multiples; in particular, 3X at approximately 147 Hz shows the highest PSD amplitude overall, followed by 9X and 6X. The spectra obtained with added trial masses of 1.5 to 3.0 U_{per} exhibit similar spectral characteristics. In the radial direction, the peak PSD magnitude initially decreases for the 1.5 and 2.0 U_{per} conditions, reaching a 50% peak reduction relative to the baseline, and then increases for the 2.5 U_{per} condition and reaches its maximum value for 3.0 U_{per}, slightly above the value for the baseline condition. This trend is particularly evident near 3X where the PSD amplitude is at its highest, but can also be observed near 6X and 9X. In the axial direction, the peak PSD magnitude decreases for the 1.5 U_{per} condition and then increases for the 2.0, 2.5 and 3.0 U_{per} conditions to reach approximately the same peak value as for the baseline condition.

Mechanical mass unbalance present in the impeller of a centrifugal pump or in the shaft assembly of a rotating machine generally produces a prominent response at 1X [7, 38]. Previous studies have also shown that structural resonances in centrifugal pumps could dominate the overall response when excited by periodic forces such as mechanical or hydraulic unbalance [11–13]. These findings are consistent with the hypothesis that the dominant response measured at 3X is amplified by a structural resonance of the pump–pipe–frame assembly. However, additional measurements of rotor unbalance and

dedicated modal testing are required to confirm this interpretation. Alternatively, the dynamic characteristics of the partially infilled 3D-printed impeller may contribute to the observed dominant 3X components, as suggested by a recent experimental study on partially infilled 3D-printed rotors [37].

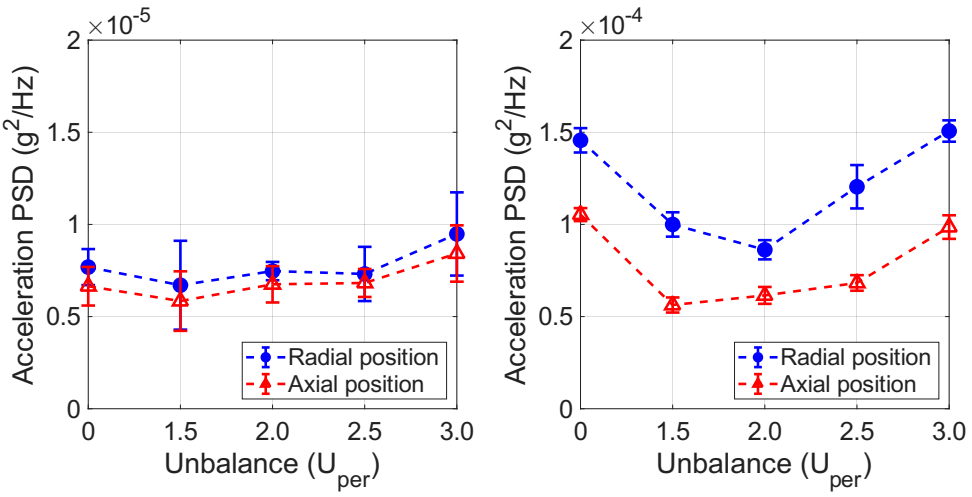
Figure 11 presents the peak PSD values for the different trial-mass conditions for 1X in (a) and 3X in (b). The peak PSD values were extracted from each individual record using the frequency-selection criteria described in Section 2.4, and the corresponding means and sample standard deviations were calculated across the five repetitions. The 3X peak PSD values are approximately one order of magnitude greater than those at 1X. The axial 1X peak PSD values, represented by the red dashed line with triangular markers in Figure 11a, initially decrease and subsequently increase as the trial mass increases. Specifically, the peak PSD values decrease by approximately 12% for the 1.5 U_{per} condition, then increase by approximately 15% for 2.0 U_{per} relative to the preceding condition, followed by an additional increase of approximately 1% for 2.5 U_{per} and finally, the largest increase relative to the preceding condition, of approximately 24%, occurs at the 3.0 U_{per} condition. The values obtained for the radial direction, represented by the blue dashed line with circular markers, exhibit a similar trend, with generally higher peak PSD values in the radial direction. The main difference is for the 2.5 U_{per} condition, where the radial peak value shows a 2% decrease relative to the preceding condition compared to the 1% increase obtained for the axial direction. It is important to note that the observed 2% change is small relative to the experimental variability represented by ± 1 standard deviation error bars. Furthermore, both curves show a similar increasing trend of the peak values when the unbalance is greater than 1.5 U_{per}.

The peak PSD values at 3X, presented in Figure 11b, show the same non-monotonic trend in the axial direction, but with larger relative changes in peak PSD magnitude. For the 1.5 U_{per} condition, the peak PSD magnitude decreases from $1.05 \times 10^{-4} \pm 6.6 \times 10^{-6}$ to $5.63 \times 10^{-5} \pm 4.1 \times 10^{-6}$ g^2/Hz (approximately 46%), and then steadily increases as larger trial masses are installed, reaching approximately the same peak PSD magnitude as in the baseline. In the radial direction, the peak PSD magnitude decreases from $1.45 \times 10^{-4} \pm 6.6 \times 10^{-6}$ to $9.99 \times 10^{-5} \pm 6.6 \times 10^{-6}$ g^2/Hz (approximately 30%) for the 1.5 U_{per} condition, and decreases by a further 14% to reach its minimum of $8.62 \times 10^{-5} \pm 5.2 \times 10^{-6}$ g^2/Hz for the 2.0 U_{per} condition. Thereafter, it increases by approximately 74% for the largest trial mass, reaching its maximum value of $1.5 \times 10^{-4} \pm 5.8 \times 10^{-6}$ g^2/Hz, just slightly higher (around 3%) than the baseline.

The prominent spectral component near 147 Hz, approximately three times the fundamental component observed near 49 Hz, is consistent with the occurrence of higher-order harmonics reported in previous investigations of additively manufactured rotors. Pinhata and Nicoletti [37] experimentally observed vibration components at 2X and 3X in FDM-manufactured shafts, particularly at reduced infill densities, and associated this behavior with printing-induced anisotropy. Their findings demonstrate that higher-order harmonics may arise in rotating systems containing additively manufactured components. However, the underlying mechanisms cannot be assumed to be identical in the present study, as here the 3D-printed component is the impeller instead

of the shaft. This means that the peak PSD amplitude near 147 Hz may involve additional dynamic interactions beyond conventional mass-unbalance excitation, which primarily occurs at the rotational frequency.

These results also suggest that the rotor assembly may exhibit residual unbalance when using the 3D-printed impeller without an added trial mass. The reduction of the PSD peak amplitude, observed at 0.135 g in the axial direction and 0.180 g in the radial direction, could be consistent with a partial compensation of an existing residual unbalance of the rotor assembly. Further increases in the added mass resulted in higher peak PSD magnitudes, which could be consistent with increasing net residual unbalance. However, this non-monotonic behavior indicates that the vibration response cannot be directly related to the magnitude of the added mass alone, highlighting the importance of considering the initial dynamic condition of the rotor–pump assembly when interpreting vibration measurements. Furthermore, because the initial residual unbalance and vibration phase were not measured, the proposed compensation mechanism remains a hypothesis, and contributions from other excitation mechanisms or structural interactions cannot be excluded.



(a) 1X (b) 3X

Fig. 11: Peak PSD values of the acceleration (mean value of five repetitions) measured for the radial (circular marker) and axial (triangular marker) directions for increasing added trial masses. Error bars represent ±1 sample standard deviation across five repetitions.

4 Conclusion

This study experimentally investigated the hydraulic performance and vibration response of a centrifugal pump equipped with a PLA impeller manufactured by fused deposition modeling. The printed impeller was designed as a replica of the original

impeller, with modifications that allowed controlled trial masses to be installed without removing the impeller from the shaft.

Dimensional measurements of five impellers manufactured using the final printing parameters showed close agreement with the original impeller and low between-specimen variability. One of these impellers was randomly selected for the hydraulic and vibration experiments. The head–flow-rate curves obtained with the original and printed impellers exhibited similar overall characteristics, with an average difference of approximately 4%. The vibration measurements at the pump inlet and outlet also showed comparable trends across the tested flow-rate range.

The dynamic response was subsequently investigated under five added trial-mass conditions, ranging from no added mass to 0.270 g at a fixed radius of 56 mm. The acceleration spectra exhibited a dominant component near 3X, the presumed third rotational harmonic, rather than at 1X, the fundamental rotational frequency. The corresponding peak PSD values initially decreased with added mass and subsequently increased. The minimum response near the third harmonic occurred at 0.135 g in the axial direction and 0.180 g in the radial direction.

The non-monotonic response may be consistent with partial compensation of an existing rotor-related excitation. However, the dominant harmonic and the reduction in vibration cannot be attributed uniquely to mass unbalance based on the present measurements. Structural resonance and the dynamic characteristics of the partially infilled printed impeller remain possible contributing mechanisms.

The results demonstrate the feasibility of using an additively manufactured impeller to investigate the influence of controlled trial masses on centrifugal-pump vibration. The proposed approach may be particularly useful for rapid prototyping and experimental evaluation of pump impellers, allowing manufacturers and research laboratories to investigate the effects of changes in mass distribution without repeatedly disassembling the rotor. The findings may also be relevant to condition-monitoring applications by highlighting the non-monotonic relationship between added mass and vibration response. However, the use of FDM-manufactured impellers in industrial pumping applications would require further validation of their mechanical durability and long-term operational performance. Future work should include direct measurement of rotor residual unbalance, modal characterization of the pump assembly, and investigation of the effects of infill density and controlled rotor balancing.

References

[1] Chen, L., Wei, L., Wang, J., Li, W.: Monitoring and predictive maintenance of centrifugal pumps based on smart sensors. Sensors **22(6)**, 1–14 (2022) https://doi.org/10.3390/s22062106

[2] Rainald, M.E., Chandran, N.S., Midhun, T.S., Akshay, M., Sreena, V.G.: IoT-driven automatic pump activation and leak detection system. In: 2025 8th International Conference on Circuit, Power Computing Technologies (ICCPCT). IEEE, Kollam (2025). https://doi.org/10.1109/ICCPCT65132.2025.11176664

[3] Werbinska-Wojciechowska, S., Rogowski, R.: Proactive maintenance of pump systems operating in the mining industry—a systematic review. Sensors **25(8)**, 1–67 (2025) https://doi.org/10.3390/s25082365

[4] Gülich, J.F.: Centrifugal Pumps, 2nd edn. Springer, Berlin (2010). https://doi.org/10.1007/978-3-642-12824-0

[5] Karassik, I., Messina, J., Cooper, P., Heald, C.: Pump Handbook, 4th edn., p. 1824. McGraw-Hill Professional, New York (2008)

[6] Lobanoff, V.S., Ross, R.R.: Centrifugal Pumps: Design and Application, 2nd edn., p. 592. Gulf Publishing Company, Houston (1992)

[7] Bently, D.E., Hatch, C.T., Grissom, B.: Fundamentals of Rotating Machinery Diagnostics, 1st edn. The American Society of Mechanical Engineers, New York (2002). https://doi.org/10.1115/1.801FRM

[8] Institute, H.: American National Standard for Rotodynamic Pumps for Vibration Measurements and Allowable Values. Hydraulic Institute Standards (2009)

[9] Wachel, J., Tison, J., Atkins, K.: Field instrumentation and diagnosis of pump vibration problems. Technical Report Rotating machinery and controls (ROMAC), University of Virginia, Virginia (1983)

[10] Birajdar, R., Keste, A.: Prediction of flow-induced vibrations due to impeller hydraulic unbalance in vertical turbine pumps using one-way fluid-structure interaction. Journal of Vibration Engineering & Technologies **8**(3), 417–430 (2019) https://doi.org/10.1007/s42417-019-00174-5

[11] Zhang, Y., Liu, J., Yang, X., Li, H., Chen, S., Lv, W., Xu, W., Zheng, J., Wang, D.: Vibration analysis of a high-pressure multistage centrifugal pump. Scientific Reports **12**(1), 20293 (2022) https://doi.org/10.1038/s41598-022-22605-2

[12] Dai, C., Zhang, Y., Pan, Q., Dong, L., Liu, H.: Study on vibration characteristics of marine centrifugal pump unit excited by different excitation sources. Journal of Marine Science and Engineering **9**(3), 274 (2021) https://doi.org/10.3390/jmse9030274

[13] Nezirić, E., Isić, S.: On some common centrifugal pumps natural frequency issues. In: Karabegovic, I., Kovačević, A., Mandzuka, S. (eds.) New Technologies, Development and Application VII vol. 1069, pp. 285–292. Springer, Cham (2024). https://doi.org/10.1007/978-3-031-66268-3_27 . Series Title: Lecture Notes in Networks and Systems

[14] Chu, T., Nguyen, T., Yoo, H., Wang, J.: A review of vibration analysis and its applications. Heliyon **10**(5), 26282 (2024) https://doi.org/10.1016/j.heliyon.2024.e26282

[15] Tiboni, M., Remino, C., Bussola, R., Amici, C.: A review on vibration-based condition monitoring of rotating machinery. Applied Sciences **12**(3) (2022) https://doi.org/10.3390/app12030972

[16] Doshi, S., Katoch, A., Suresh, A., Razak, F.A., Datta, S., Madhavan, S., Zanhar, C.M., Gundabattini, E.: A review on vibrations in various turbomachines such as fans, compressors, turbines and pumps. Journal of Vibration Engineering & Technologies **9**(7), 1557–1575 (2021) https://doi.org/10.1007/s42417-021-00313-x

[17] MacCamhaoil, M.: Static and dynamic balancing of rigid rotors. Report, Brüel & Kjaer (1988)

[18] Manni, G.: Balancing Theory and Application, 2.1 edn. CEMB SpA, Mandello del Lario (1999)

[19] Bai, L., Zhou, L., Jiang, X., Pang, Q., Ye, D., Tusset, A.M.: Vibration in a multistage centrifugal pump under varied conditions. Shock and Vibration **2019**(1) (2019) https://doi.org/10.1155/2019/2057031

[20] Nakazawa, T., Makinouchi, K., Takami, Y., Glueck, J., Tayama, E., Nosé, Y.: Vibration assessment for thrombus formation in the centrifugal pump. Artificial Organs **21**(4), 318–322 (1997) https://doi.org/10.1111/j.1525-1594.1997.tb00368.x

[21] Prashar, G., Vasudev, H., Bhuddhi, D.: Additive manufacturing: expanding 3D printing horizon in industry 4.0. International Journal on Interactive Design and Manufacturing (IJIDeM) **17**(5), 2221–2235 (2023) https://doi.org/10.1007/s12008-022-00956-4

[22] Babayiğit, O., Sefaci, S., Şahbaz, M.: Usage of 3D printing technology in centrifugal pumps and material selection. Proceedings of the Institution of Mechanical Engineers, Part C: Journal of Mechanical Engineering Science **238**(3), 837–848 (2023) https://doi.org/10.1177/09544062231175789

[23] Fernández, S., Jiménez, M., Porras, J., Romero, L., Espinosa, M.M., Domínguez, M.: Additive manufacturing and performance of functional hydraulic pump impellers in fused deposition modeling technology. Journal of Mechanical Design **138**(2) (2016) https://doi.org/10.1115/1.4032089

[24] Polák, M.: Behaviour of 3D printed impellers in performance tests of hydrodynamic pump. In: Proceeding of 7th International Conference on Trends in Agricultural Engineering 2019, Prague, pp. 447–452 (2019)

[25] Mansour, G., Papageorgiou, V., Tzetzis, D.: Carbon fiber polymer reinforced 3D printed composites for centrifugal pump impeller manufacturing. Technologies **12**(4), 48 (2024) https://doi.org/10.3390/technologies12040048

[26] Subramani, R.: Optimizing process parameters for enhanced mechanical performance in 3D printed impellers using graphene-reinforced polylactic acid (g-PLA) filament. Journal of Mechanical Science and Technology **39**(3), 1387–1397 (2025) https://doi.org/10.1007/s12206-025-0231-4

[27] Pinhata, G.M., Nicoletti, R.: The dynamics of a 3D printed microrotor. The International Journal of Advanced Manufacturing Technology **121**(3), 2803–2814 (2022) https://doi.org/10.1007/s00170-022-09454-z

[28] Joswig, L., Vellekoop, M.J., Lucklum, F.: Miniature 3D-printed centrifugal pump with non-contact electromagnetic actuation. Micromachines (Basel) **10**(10) (2019) https://doi.org/10.3390/mi10100631

[29] Jayawardane, H., Davies, I.J., Gamage, J.R., John, M., Biswas, W.K.: Investigating the 'techno-eco-efficiency' performance of pump impellers: metal 3D printing vs. CNC machining. The International Journal of Advanced Manufacturing Technology **121**(9-10), 6811–6836 (2022) https://doi.org/10.1007/s00170-022-09748-2

[30] Remache, A., Pérez-Sánchez, M., Hidalgo, V.H., Ramos, H.M., Sánchez-Romero, F.-J.: Towards sustainability in hydraulic machinery manufacturing by 3D printing. Processes **12**(12), 2664 (2024) https://doi.org/10.3390/pr12122664

[31] Cantrak, D.S., Jankovic, N.Z., Ilic, D.B., Lecic, M.R.: Centrifugal pumps' impellers design and digital fabrication. In: 1st International Conference Multidisciplinary Engineering Design Optimization (MEDO). IEEE, New York (2016)

[32] Jia, D., Li, F., Zhang, Y.: 3D-printing process design of lattice compressor impeller based on residual stress and deformation. Scientific Reports **10**(1), 600 (2020) https://doi.org/10.1038/s41598-019-57131-1

[33] Andres, N.S.: Development of solar-powered water pump with 3D printed impeller. Open Engineering **11**(1), 249–253 (2021) https://doi.org/10.1515/eng-2021-0015

[34] Kong, J.-R., Kim, H.-J.: Dimensional characteristics of impeller output using 3D printers. Journal of the Korean Society of Manufacturing Process Engineers **21**(9), 56–62 (2022) https://doi.org/10.14775/ksmpe.2022.21.09.056

[35] Qu, A., Li, F.: Effect of double crack on fatigue crack growth life of 3D printing compressor impeller. Thin-Walled Structures **189**, 110883 (2023) https://doi.org/10.1016/j.tws.2023.110883

[36] Qu, A., Li, F.: Influence of 3D printing on compressor impeller fatigue crack propagation life. International Journal of Mechanical Sciences **245** (2023) https://doi.org/10.1016/j.ijmecsci.2023.108107

[37] Pinhata, G.M., Nicoletti, R.: Experimental analysis of the dynamic response of 3D-printed rotors. The International Journal of Advanced Manufacturing Technology **139**, 4815–4827 (2025) https://doi.org/10.1007/s00170-025-16051-3

[38] Rao, B.K.N.: Handbook of Condition Monitoring, 1st edn. Elsevier Advanced Technology, Oxford (1996)

Statements and Declarations

Funding

L. Enrique Ortiz-Vidal gratefully acknowledges the support of the Agencia Nacional de Investigación y Desarrollo (ANID-Chile) for Fondecyt grant 11240690. Partial funding for this work was received from project FIC 40048425-0 "Transferencia fabricación digital para jóvenes makers".

Competing interests

All authors certify that they have no affiliations with or involvement in any organization or entity with any financial interest or non-financial interest in the subject matter or materials discussed in this manuscript.

Author contributions

All authors contributed to the study conception and design. Material preparation, data collection and preliminary analysis were performed by Sebastian Jeldres and Enrique Ortiz-Vidal, while the final analysis was performed by Daniel Casagrande. The first draft of the manuscript was written by Daniel Casagrande and all authors commented on previous versions of the manuscript. All authors read and approved the final manuscript.